Dynamic Simulation of the Imbalance Netting Process and Cross-Border Activation of the automatic Frequency Restoration Process

Marcel Topler, Boštjan Polajžer

University of Maribor, Faculty of Electrical Engineering and Computer Science, Koroška cesta 46, 2000 Maribor, Slovenia, +386 2 22 07 340, marcel.topler@um.si; +386 2 22 07 076, bostjan.polajzer@um.si

Abstract: This paper discusses the Imbalance Netting Process (INP) and cross-border activation of the automatic Frequency Restoration Process (aFRP) between interconnected Control Areas (CAs). The primary goal of INP is to net the demand for balancing energy between participating CAs with different signs of interchange power variation. In this way, the INP reduces the amount of activated regulating reserve. Moreover, frequency quality should also be improved. Due to the new network codes, INP will be developed further in a way that will enable cross-border activation of the aFRP. However, contrary to INP, cross-border activation of aFRP is possible only between CAs with equal signs of interchange power variation. Therefore, the impact of INP and cross-border activation of aFRP on frequency quality and provision of Load-Frequency Control (LFC) is analyzed thoroughly. The obtained results confirm that INP, as well as cross-border activation of aFRP, reduce balancing energy and, consequently, release regulating reserve. In addition, the unintended exchange of energy is also reduced. Furthermore, the obtained results also indicate the impact of INP and cross-border activation of aFRP on the performance of the frequency control.

Keywords: Frequency quality, Load-Frequency Control, imbalance netting, frequency restoration, regulating reserve, cross-border

1 Introduction

One of the main tasks of a Transmission System Operator (TSO) is to maintain the balance between production and consumption of electrical energy in its Control Area (CA) [1]. The imbalances are reflected in the frequency deviation, which must stay within different target values. Therefore, the frequency is regulated at different levels, i.e., primary and secondary. According to new network codes, primary control is also known as the Frequency Containment Process (FCP), whereas secondary control is known as automatic Frequency Restoration Process (aFRP), i.e., Load-Frequency Control (LFC) [2] – [4]. The Imbalance Netting Process (INP) was developed in order to avoid the simultaneous activation of regulating reserves with different signs. In this way, CAs with excess of energy can compensate CAs with a deficit of energy, and vice versa. The structure of INP adds a correction value to the calculation of Area Control Error (ACE) through a virtual tie-line, including actual responses of control units. Resulting from the reduced amount of activated regulating reserve, INP also reduces financial costs [5]. New network codes require further cost optimization, therefore INP will be developed further in a way that will enable cross-border activation of the automatic Frequency Restoration Process (aFRP). In this way, greater economic and technical efficiency of the participating CAs will be provided [6].

Frequency quality has been declining in recent years [7], and INP, as well as cross-border activation of aFRP, are expected to have a positive impact on its quality, and on the provision of LFC. In [5] it is shown that INP releases regulating reserve without impact on the provision of LFC. The basic structure of cross-border activation of aFRP is given in [8].

2 LFC, INP and Cross-Border Activation of aFRP

2.1 Basic Principle of LFC

Each TSO provides LFC in its CA, which reduces the frequency deviations and interchange power variations on the connecting tie-lines. Frequency deviation and interchange power variation of the *i*-th CA are defined as

$$\Delta f_i = f_{\mathrm{a}i} - f_{\mathrm{s}i}$$

and

$$\Delta P_i = P_{\mathrm{a}i} - P_{\mathrm{s}i} \,,$$

respectively. Here, $f_{\mathrm{a}i}$ and $P_{\mathrm{a}i}$ denote actual, i.e., measured values, whereas $f_{\mathrm{s}i}$ and $P_{\mathrm{s}i}$ denote scheduled values. The imbalance between production and consumption of the *i*-th CA is measured by an ACE as

$$ACE_i' = \Delta P_i + B_i \Delta f_i \,,$$

where B_i is the frequency bias coefficient that reflects the CAs size. Note that ACE_i' does not include a correction term due to INP.

The basic LFC structure for the *i*-th CA is shown in Figure 1 with a solid line, where SH denotes Sample and Hold with a sampling time T_{s}, LPF is a Low-Pass Filter, and PI is a Proportional-Integral Controller. A negative control-feedback is included as -1 gain. The output of LFC is scheduled control power $\Delta P_{\mathrm{sc}i}$, which is distributed between the different control units that participate in LFC. The sum of active electric power of the individual control units, which change active electric power accordingly, is denoted as $\Delta P_{\mathrm{e}i}$.

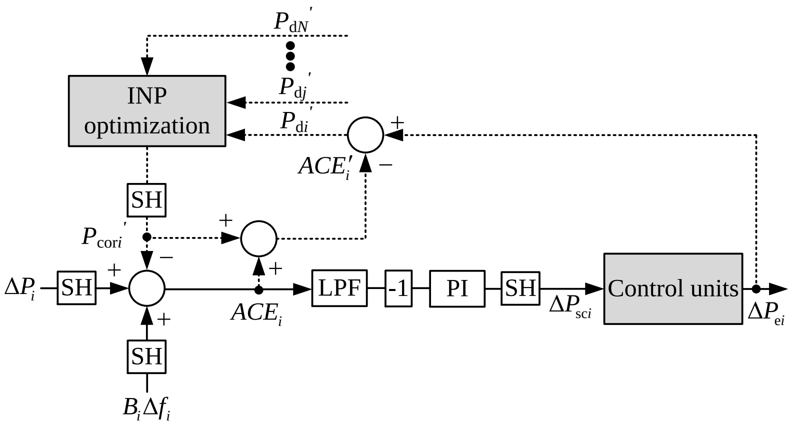

Figure 1: Block diagram of LFC (solid line) with INP optimization (dotted line) of the i-th CA.

2.2 Basic Principle of INP

INP was implemented in order to reduce the amount of activated regulating reserve and the associated financial costs for balancing energy. Thus, CAs with opposite signs of power variations can compensate those variations with the participating CAs. In this way, balancing energy can be reduced, while regulating reserve can be released. The input variable for INP is demand power $P_{\mathrm{d}i}'$, that determines the total power to be compensated with other CAs that have the opposite sign of ACE_i'. Note, negative ACE_i' means that the production is lower than the consumption, consequently, CA is “short”. Therefore, a positive $P_{\mathrm{d}i}'$ is required for the increase of ACE_i'. Positive ACE_i' means that CA is “long”, and $P_{\mathrm{d}i}'$ should be negative. Thus, the demand power is given as

$$P_{\mathrm{d}i}' = \Delta P_{\mathrm{e}i} - ACE_i' .$$

Furthermore, the INP output variable is a correction power $P_{\mathrm{cor}i}'$, and is incorporated as

$$ACE_i = \left(\Delta P_i + B_i \Delta f_i\right) - P_{\mathrm{cor}i}' ,$$

where terms in brackets denote ACE_i'. Obviously, $P_{\mathrm{cor}i}'$ and $P_{\mathrm{d}i}'$ must have opposite signs. The structure of LFC with INP is shown in Figure 1 with a dotted line, where the INP optimization module provides $P_{\mathrm{cor}i}'$ with a time delay T_{s} due to SH.

2.2.1 INP Optimization

The main objective of INP optimization is the maximal possible compensation with a general limit of $P_{\mathrm{d}i}'$ and the limit of Available Transmission Capacity (ATC). Note that the limit of ATC can differ for each direction of compensation. When connecting more CAs together through one common point, a target function of fairness must be considered, which distributes $P_{\mathrm{cor}i}'$ between CAs. Commonly, a proportional to imbalance distribution is used [9]. If parallel transmission lines are available, a target function should be considered of advantageous use of transmission lines with the highest ATC. Note that this paper does not consider INP optimization, although proportional to imbalance distribution is used.

2.3 Basic Principle of Cross-Border Activation of aFRP

Due to the new network codes, which require additional cost optimization, INP will be developed further in a way that will enable cross-border activation of aFRP. TSOs agreed to use the control demand approach for the cross-border activation of aFRP, which is the same approach as currently used for INP, and is shown schematically in Figure 2 [6]. Similarly to INP, the input variable for aFRP optimization is demand power $P_{\mathrm{d}i}^*$, that determines the total power to be compensated. However, unlike INP, the compensation for cross-border activation of aFRP is possible between CAs that have equal signs of ACE_i'. The demand power is given as

$$P_{\mathrm{d}i}^* = \Delta P_{\mathrm{e}i} - ACE_i^* .$$

Furthermore, the INP output variable is a correction power $P_{\mathrm{cor}i}^*$ and is incorporated as

$$ACE_i^* = \left(\Delta P_i + B_i \Delta f_i\right) - P_{\mathrm{cor}i}^* - K_j \cdot P_{\mathrm{cor}j}^* ,$$

where terms in brackets denote ACE_i'. Note that P_{corj}^* is correction power from the j-th CA, that is activated in the i-th CA. In addition, factor K_j is the ammount of P_{corj}^* activated in the i-th CA, where 1 means 100 %. The structure of LFC with cross-border activation of aFRP is shown in Figure 2 with a dotted line, where the aFRP optimization module provides P_{cori}^* with a time delay T_s due to SH.

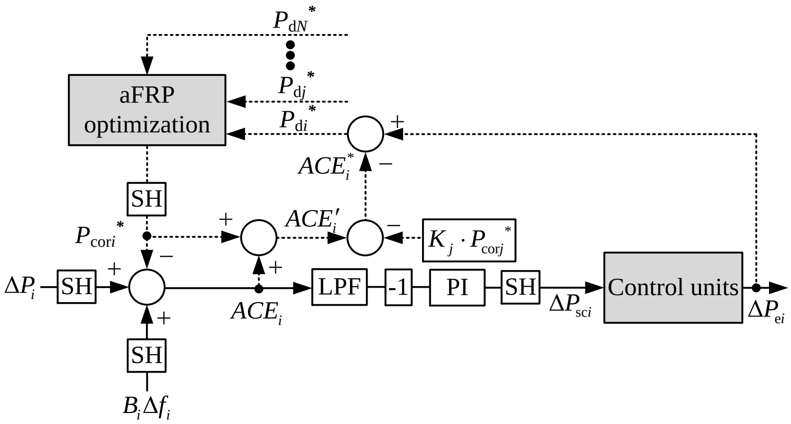

Figure 2: Block diagram of LFC (solid line) with aFRP optimization (dotted line) of the i-th CA.

2.3.1 AFRP Optimization

The main taget function of aFRP optimization is the maximal possible compensation with a general limit of P_{di}^*. The objective is to control ACE_i' to zero, therefore, the amount of P_{cori}^* to be activated should cover P_{di}^*. Furthermore, the amount of activated P_{cori}^* in the i-th CA should be minimized, and should be activated in the j-th CA. Generally, the most economic efficient bids of P_{cori}^* activation should be chosen. In addition, the limit of ATC should also be considered.

2.4 Steady-State Examples

2.4.1 INP Based Correction

Steady-state values of INP based correction are shown in Figure 3, where CA_1 and CA_3 are connected only with a virtual tie-line through the INP optimization module. However, they are not connected physically. In the discussed example, CA_1 and CA_2 are long (P_{d1} = – 60 MW, P_{d2} = – 40 MW), while CA_3 is short (P_{d3} = + 80 MW). Without limited ATC, CA_3 imports 80 MW, which is distributed between CA_1 and CA_2 proportionally to their imbalances. Thus CA_1 exports 48 MW, while CA_2 exports 32 MW. Consequently, CA_1 and CA_2 both remain long ($P_{d1} + P_{cor1}$ = – 12 MW, $P_{d2} + P_{cor2}$ = – 8 MW), while CA_3 is balanced ($P_{d3} + P_{cor3}$ = 0 MW). In the case of limited ATC for INP power interchange with P_{atc12} = 30 MW and P_{atc23} = 70 MW, CA_3 can import only 70 MW. Therefore, CA3 remains short ($P_{d3} + P_{cor3}$ = + 10MW), CA_1 is long ($P_{d1} + P_{cor1}$ = – 30 MW) and CA_2 is balanced ($P_{d2} + P_{cor2}$ = 0 MW).

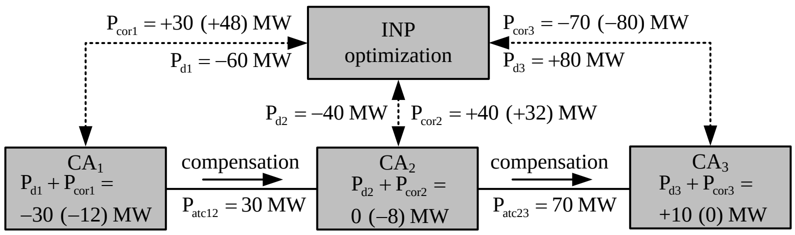

Figure 3: Steady-state correction value calculation with INP optimization, where results without ATC limits are represented in brackets.

2.4.2 Cross-Border Activation of aFRP Based Correction

Steady-state values of aFRP based correction are shown in Figure 4, where CA_1 and CA_3 are connected only with a virtual tie-line through the aFRP optimization module, although , they are not connected physically. In the discussed example, CA_1, CA_2 and CA_3 are short (P_{d1} = + 40 MW, P_{d2} = + 60 MW and P_{d3} = + 80 MW). Without limited ATC, CA_3 activates +24 MW in CA_1 and +56 MW in CA_2, thus imports P_{cor3} = +80 MW. Consequently, CA_3 is balanced ($P_{d3} + P_{cor3}$ = 0 MW). In the case of limited ATC for aFRP power interchange with P_{atc12} = 30 MW and P_{atc23} = 70 MW, CA_3 can import only 70 MW. Therefore, CA_3 activates +30 MW in CA_1 and +40 MW in CA_2. In this way, CA_3 remains short ($P_{d3} + P_{cor3}$ = +10 MW).

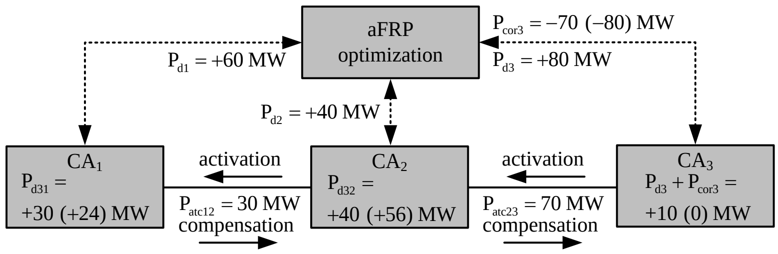

Figure 4: Steady-state correction value calculation with aFRP optimization, where results without ATC limits are represented in brackets.

3 Dynamic Simulations

A testing system with three identical CAs was modeled, where CA_1–CA_2 and CA_2–CA_3 were connected with tie-lines, whereas CA_1–CA_3 were not connected physically, as shown in Figures 3 and 4. In addition, all three CAs were connected by the INP or aFRP optimization module through virtual tie-lines separately. A Matlab/SIMULINK model was developed, where numerical simulations were performed using a 50 ms step-size.

3.1 Dynamic Model

3.1.1 Structure

An individual CA was described with a linearized low-order model, and is shown schematically in Figure 5 [9]. It is assumed that voltage control (reactive power) does not impact frequency control (active power). Moreover, a group of several generators was replaced with one equivalent, where the electrical part is ignored and generator dynamics are represented by rotor inertia H_i and damping D_i. Three different types of governor-turbine systems were considered, i.e., hydraulic, steam reheat and steam non-reheat. In addition, a constant droop characteristic R_i was assumed. Tie-line connections with various CAs were described by synchronizing coefficient T_{ij} that is defined with parameters of a lossless equivalent tie-line in the vicinity of the operating point. In addition, a 1-st order LPF and PI controller were modeled, as well as ramping rate and participation factors α_i of control units.

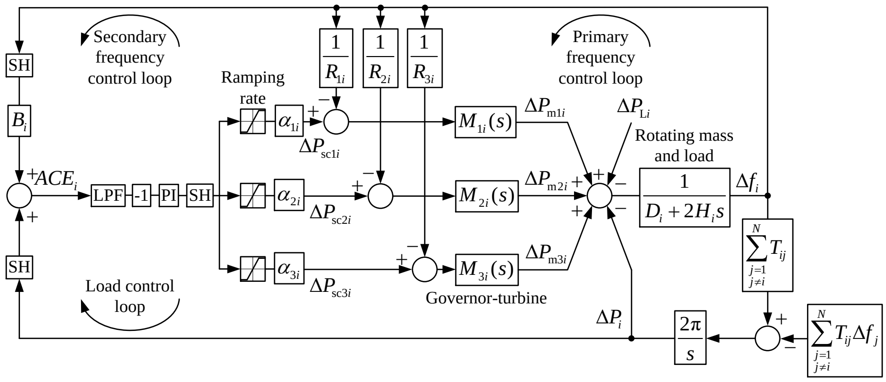

Figure 5: Block diagram of a single i-th CA.

3.1.2 Parameters

Typical values of parameters were set for the testing system [1], [11]. Gain and time constants of LPFs were set as $K_{\mathrm{LPF}i} = 1$ and $T_{\mathrm{LPF}i} = 15$ s, whereas the gain of the PI controller was set as $K_{\mathrm{PI}i} = 0{,}3$. Equal participation factors were set, i.e., $\alpha_{1i} = \alpha_{2i} = \alpha_{3i} = 1/3$. Frequency bias was determined as $B_i = (1/R_i + D_i)$, where $D_i = 0{,}01$ pu/Hz, $1/R_i = 1/R_{1i} + 1/R_{2i} + 1/R_{3i}$ and $R_{1i} = R_{2i} = R_{3i} = 3$ Hz/pu. Furthermore, $H_i = 0{,}1$ pu s, whereas $T_{ij} = 0{,}033$ pu/Hz, which is for strongly coupled systems. The rate limit for the steam reheat turbine was set to ± 10 puMW/min, the steam non-reheat turbine to ± 20 puMW/min, and the hydraulic turbine to ± 100 puMW/min. The model parameters were equal for all three CAs, and the only differences were PI controller time constants $T_{\mathrm{PI}i}$, which have the biggest impact on frequency response. They were set as $T_{\mathrm{PI}1} = 60$ s, $T_{\mathrm{PI}2} = T_{\mathrm{PI}3} = 30$ s. Note that one cycle of LFC, INP and cross-border activation of aFRP was incorporated by $T_{\mathrm{s}} = 2$ s.

3.2 Testing Cases

Dynamic simulations were performed separately for the system with INP and separately for the system with aFRP. In addition, the limit of ATC power was not considered. In order to evaluate the impact of INP and cross-border activation of aFRP on LFC performance, the loads of individual CAs were changed simultaneously, and their proportions were maintained through the entire simulation. For step change of ΔP_{Li} used in numerical simulations for three CAs with INP, two cases were considered. For Case 1, load magnitudes were set so that CA_1 and CA_2 were long, while CA_3 was short, whereas for Case 2, CA_1 was short, while CA_2 and CA_3 were long. Moreover, the absolute value of the sum of loads in long CAs was higher than the absolute value of load in the short CA, which enabled full compensation.

Two cases were also considered for the step change of ΔP_{Li} used in numerical simulations for three CAs with cross-border activation of aFRP. However, for Case 1, load magnitudes were set so that CA_1, CA_2 and CA_3 were short, whereas for Case 2, CA_1, CA_2 and CA_3 were long. In this way, cross-border activation of aFRP in all three CAs was possible. In addition, in both cases, CA_3 activated $0.3P_{corj}^*$ in CA_1 and $0.7P_{corj}^*$ in CA_2. The resulting loads are seen in Figure 6. Note that the numerical simulations were performed separately for the system with INP and separately for the system with aFRP.

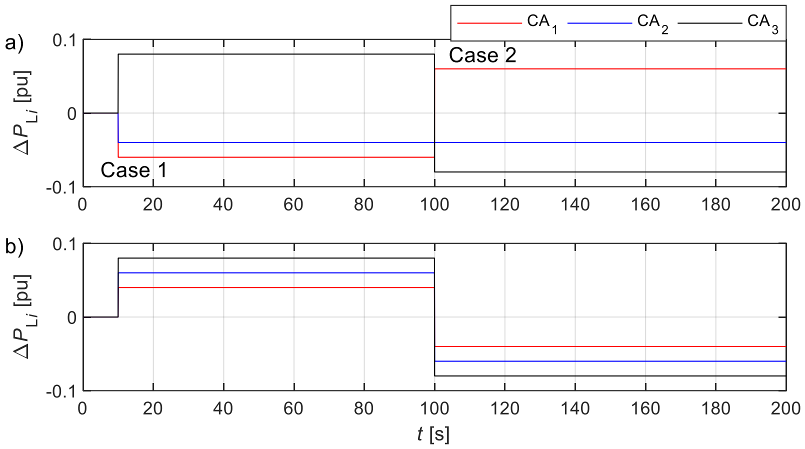

Figure 6: Step change of ΔP_{Li} used in numerical simulations for three CAs with INP (a) and with cross-border activation of aFRP (b).

4 Results

Dynamic simulations were performed for a three CA testing system in order to analyze the impact of INP and cross-border activation of aFRP on the system's response. The impact was evaluated according to the obtained results.

4.1 Time Responses to Step Changes of Loads With INP

Results are shown in Figure 7 and 8. When a step change of load is applied, frequency deviations Δf_i in all three CAs occur, as shown in Figure 7 – left. In Case 1, Δf_i is positive, due to the negative value of the total load change, i.e., $\Sigma\Delta P_{Li} = -0.02$ pu. Furthermore, the first peak of Δf_3 is negative, due to the positive value of ΔP_{L3}. Initially, primary frequency control reduces Δf_i in approximately 30 s after the step change, then, additionally, LFC decreased Δf_i slowly. Responses in Case 2 are similar, however $\Sigma\Delta P_{Li} = -0.06$ pu and the first peak of Δf_1 is negative due to the positive value of ΔP_{L1}. The obtained results show that INP impacts Δf_i, but only after the completion of the primary response. It is shown clearly that INP has reduced Δf_i in all three CAs in Case 1. However, in Case 2, the absolute value of Δf_2 and Δf_3 was increased. The impact of INP is shown more clearly in Figure 7 – right and Figure 8 – left. In all three CAs, ACE_i, ΔP_{sci} and ΔP_{ei} were reduced due to INP. However, INP has obviously increased ΔP_i due to the tie-line power flow for compensation between CAs. The signs of P_{di} and P_{cori} are opposite, as shown in Figure 8 – right, and a time delay of 2 s is noticed in P_{cori}, especially at the beginning of both transients. Moreover, due to the oscillations of Δf_i, a sign change is noticed in P_{di}. Consequently, P_{cori} also changes sign, and can also be zero. Therefore, the fast changing compensations are not desirable, since they increase variations in ACE_i, as shown in Figure 7 – right. Note that steady-state corrrection values with INP for Case 1 are shown in Figure 3.

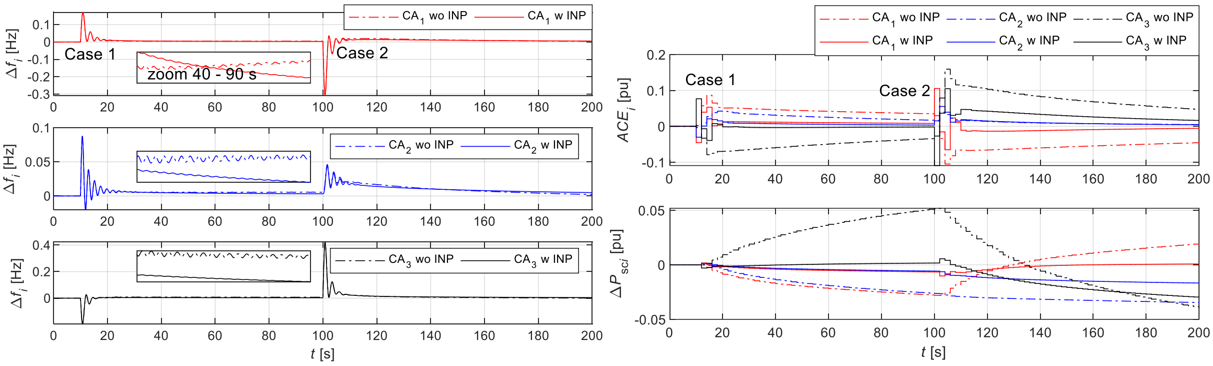

Figure 7: Time response of Δf_i, ACE_i and ΔP_{sci} for a three CA testing system, where "wo" is without INP and "w" is with INP.

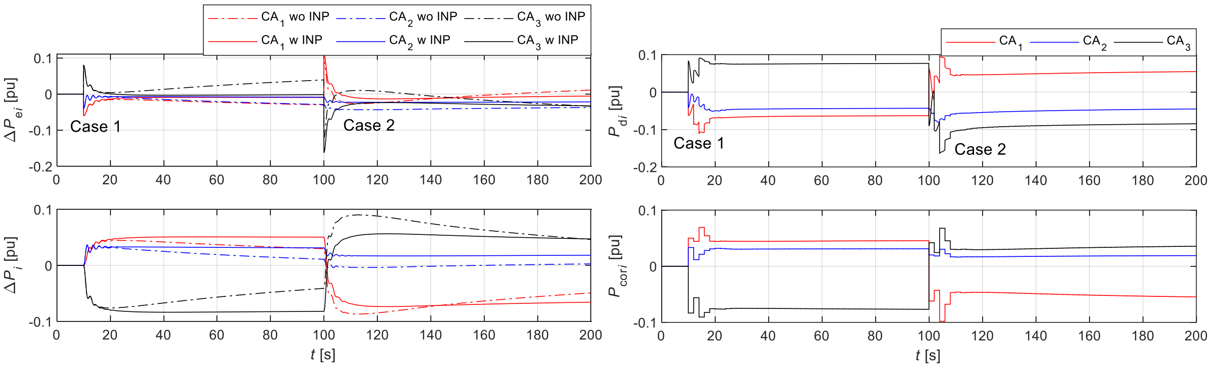

Figure 8: Time response of ΔP_{ei}, ΔP_i, P_{di} and P_{cori} for a three CA testing system, where "wo" is without INP and "w" is with INP.

4.2 Time Responses to Step Changes of Loads With Cross-Border Activation of aFRP

Results are shown in Figures 9 and 10. When a step change of load is applied, Δf_i occurs in all three CAs, as shown in Figure 9 – left. In Case 1, Δf_i is negative due to the positive value of the total load change, i.e., $\Sigma\Delta P_{Li}$ = +0.18 pu. Initially, primary frequency control reduces Δf_i in approximately 30 s after the step change, then, additionally, LFC decreased Δf_i slowly. Responses in Case 2 are similar, only the signs are different due to the $\Sigma\Delta P_{Li}$ = –0.18 pu. The obtained results show that cross-border activation of aFRP impacts Δf_i, but only after the completion of the primary response. It is shown clearly that cross-border activation of aFRP has reduced Δf_i in all three CAs, both in Case 1 and 2. The impact of cross-border activation of aFRP is shown more clearly in Figure 9 – right and Figure 10 – left. In all three CAs, ACE_1 and ACE_2 were increased, whereas ACE_3 was reduced, because CA_3 activated $0.3P_{corj}^*$ in CA_1 and $0.7P_{corj}^*$ in CA_2. Therefore ACE_3 changed sign. Consequently, ΔP_{sc1}, ΔP_{sc2}, ΔP_{e1} and ΔP_{e2} were also increased, whereas ΔP_{sc3} and ΔP_{e3} were reduced or changed sign. However, cross-border activation of aFRP has obviously increased ΔP_i due to the increased tie-line power flow. The signs of P_{di} and P_{cori} are opposite, as shown in Figure 10 – right, and a time delay of 2 s is noticed in P_{cori}, especially at the beginning of both transients. Note that steady-state corrrection values with aFRP for Case 1 are shown in Figure 4.

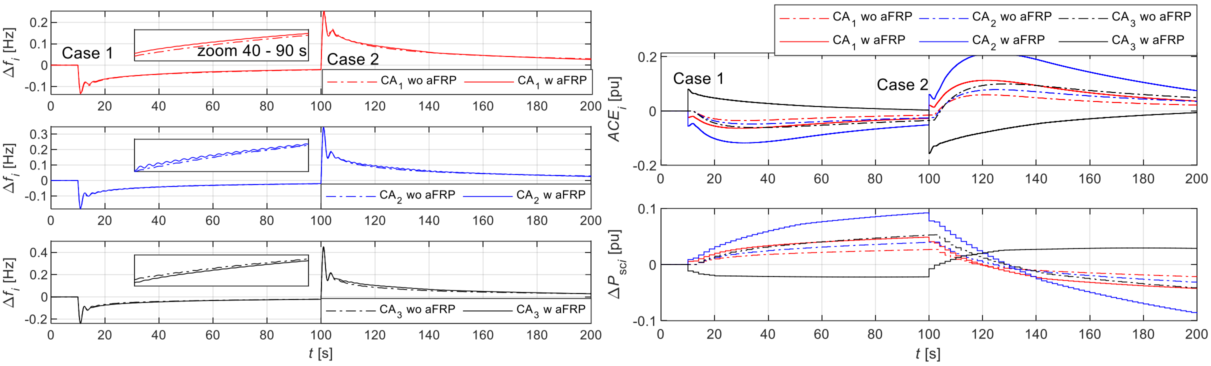

Figure 9: Time response of Δf_i, ACE_i and ΔP_{sci} for a three CA testing system, where "wo" is without aFRP and "w" is with aFRP.

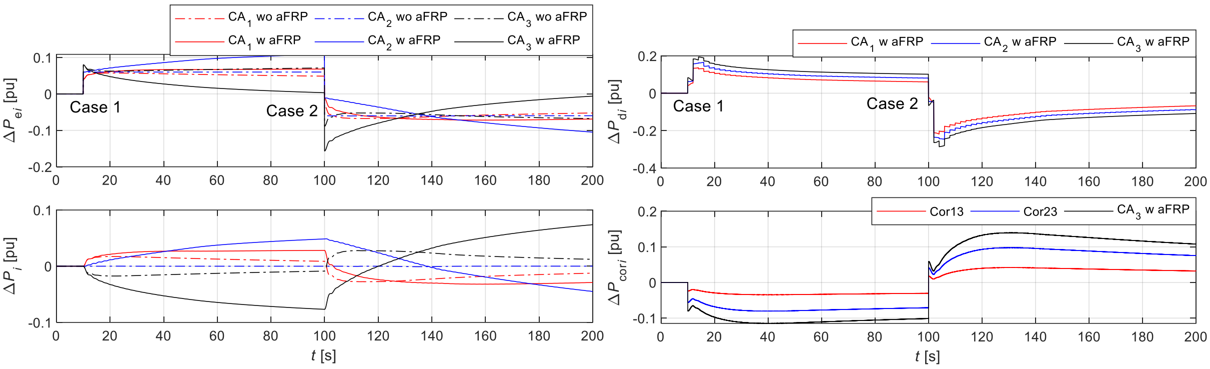

Figure 10: Time response of ΔP_{ei}, ΔP_i, P_{di} and P_{cori} for a three CA testing system, where "wo" is without aFRP and "w" is with aFRP. Note, "Cor13" is P_{cori} from CA_1 to CA_3 and "Cor23" is P_{cori} from CA_2 to CA_3.

5 Conclusion

The impact of INP and cross-border activation of aFRP on frequency quality and provision of LFC in a three CA testing system was shown in this paper. For a three CA testing system, dynamic simulations were performed with step changes of loads. From the obtained results it can be concluded that INP, as well as cross-border activation of aFRP, decrease the frequency deviation, but cases of frequency deterioration also exist. It should be emphasized that INP and cross-border activation of aFRP have an impact on LFC, although the impact on Primary Frequency Control is not evident from the results. Moreover, ACE_i, ΔP_{sci} and ΔP_{ei} were decreased with INP. In cases of frequency oscillations, INP might generate increased variations in ACE_i, therefore, fast changing compensations are not desirable. In addition, smaller activation of secondary control reserve is needed, therefore, INP releases regulating reserve and reduces balancing energy. Cross-border activation of aFRP decreased ACE_i, ΔP_{sci} and ΔP_{ei} in cases, when CA_j activated P_{corj}^* in CA_i, and vice versa. Consequently, smaller activation of secondary control reserve is needed in CA_j, therefore, also, cross-border activation of aFRP releases regulating reserve and reduces balancing energy.

Future work should focus on the dynamic dimensioning of regulating reserves with respect to INP and cross-border activation of aFRP. In this way, possible over dimension of regulating reserve could be decreased.

6 References

[1] P. Kundur, “Power system stability and control.” New York: McGraw-Hill, 1994.

[2] *Establishing a guideline on electricity transmission system operation*, Commission Regulation (EU) 2017/1485, Aug. 2017.

[3] *Frequency response standard*, background document, NERC, Nov. 2012.

[4] N. Jaleeli and L. S. VanSlyck, “NERC’s new control performance standards.” IEEE Trans. Power Syst., vol. 14, no. 3, pp. 1092—1099, Aug. 1999.

[5] P. Zolotarev et.al., “Grid Control Cooperation – A framework for technical and economical cross border optimization for load-frequency control.” In Proceedings of the 44th International Conference on Large High Voltage Electric Systems (Cigre’12), Paris, France, 26–30 Aug. 2012.

[6] *Proposal for the implementation framework for a European platform for the exchange of balancing energy from frequency restoration reserves*, ENTSO-E, Brussels, Belgium, Apr. 2012.

[7] *Operational Reserve Ad Hoc Team Report*, ENTSO-E, Brussels, Belgium, May 2012.

[8] Consultation on the design of the platform for automatic Frequency Restoration Reserve (aFRR) of PICASSO region, ENTSO-E, Brussels, Belgium, Nov. 2012.

[9] M. Scherer and G. Andersson, “A blueprint for the imbalance netting process using multi-objective optimization.” IEEE International Energy Conference (ENERGYCON), Belgium, Apr. 2016.

[10] P. M. Anderson and M. Mirheydar, “A low-order system frequency response model.” IEEE Trans. Power Syst., vol. 5, no. 3, pp. 720-729, Aug. 1990.

[11] H. Bevrani, “Robust power system frequency control.” New York: Springer, 2009.